# Effects of Oxidizing/Reducing Agent Ratio on Phase Purity, Crystallinity, and Magnetic Behavior of Solution-Combustion-Grown BiFeO₃ Submicroparticles

José-Luis Ortiz-Quiñonez,[‡] Umapada Pal,*,[†] and Martin Salazar Villanueva[‡]

[†]Instituto de Física, Benemérita Universidad Autónoma de Puebla, Apartado Postal J-48, 72570 Puebla, Puebla, Mexico
[‡]Facultad de Ingeniería, Benemérita Universidad Autónoma de Puebla, Apartado Postal J-39, 72570 Puebla, Puebla, Mexico

ABSTRACT: Fabrication of phase-pure well-crystalline BiFeO₃ submicroparticles in large scale is of great importance for the utilization of this rhombohedrally distorted perovskite material in applications such as memory storage and spintronic devices and visible photocatalyst for the degradation of organic pollutants. In fact, because of the narrow temperature range of phase stabilization, the fabrication of phase-pure BiFeO₃ in large scale remained elusive. We present the synthesis of phase-pure BiFeO₃ particles of submicrometric dimensions (246−330 nm average size) through the adjustment of oxidizing/reducing agent ratio in solution combustion process utilizing glycine as reducing agent and nitrate precursors as oxidizing agent. Utilizing X-ray diffraction and Raman spectroscopy, we demonstrate that the BiFeO₃ submicroparticles synthesized at equivalence ratio (Φ_e) close to 0.5 do not contain undesired impurities such as Bi₂Fe₄O₉ and Bi₂₄Fe₂O₃₉. Moreover, the submicroparticles are highly crystalline, possessing high room temperature magnetic moment and stable antiferromagnetic behavior across a wide temperature range. The superparamagnetic behavior at low magnetic field manifested by impurities attached to the BiFeO₃ submicroparticles might lead to their use as effective magnetically separable photocatalysts.
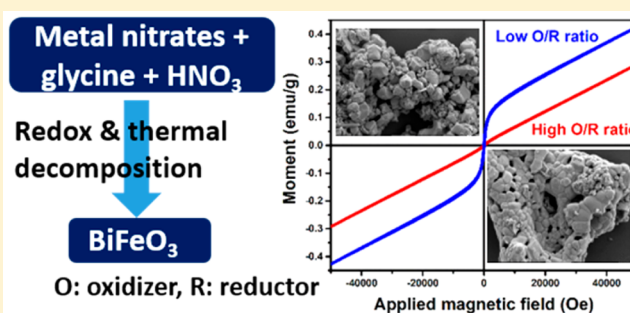
1. INTRODUCTION

Bismuth ferrite is an interesting material due to its magnetic and ferroelectric behaviors at room temperature. Whereas Catalan and Scott[1] have nicely summarized the general physical properties and possible applications of BiFeO₃, other uses of BiFeO₃ include the degradation of organic pollutants[2,3] and catalyst in the synthesis of dihydro-2-oxypyrroles.[4] Bulk BiFeO₃ is an antiferromagnetic material with Néel temperature around 635 K.[1,5] Each Fe^{3+} spin in BiFeO₃ is surrounded by six antiparallel spins of the nearest Fe neighbors.[1] The spins are not perfectly antiparallel, as there is a weak canting moment caused by the local magnetoelectric coupling to the polarization.[1] Superimposed on this canting is a cycloidal spiral of the antiferromagnetically ordered sublattices, with a period of ∼62 nm.[6] Also, on decreasing size, the BiFeO₃ particles become slightly ferromagnetic.[7]

There are several synthesis methods to obtain BiFeO₃ particles such as hydrothermal,[2] microwave-assisted hydrothermal,[8] coprecipitation followed by calcination,[9] solution combustion reactions using different chelating agents (citric acid, sucrose, urea, tartaric acid, glycine) followed by calcination,[4,10,11] solid-state reactions,[3] and sol−gel processes.[12] The main drawback or inconvenience with those methods is the formation of impurities, which in many cases are in considerable concentrations, to be clearly detected by X-ray diffraction, such as Bi₂Fe₄O₉,[3,4,8,9,12] Bi₂₄Fe₂O₃₉,[3,8,9,12] Bi₂₅FeO₄₀,[2] Bi₃₆Fe₂₄O₅₇,[4] or trapped nitrates.[8] While the

solution combustion process is an easier method for synthesizing BiFeO₃ submicroparticles on the large scale, the presence of impurities does not allow one to obtain reliable values of the measured properties of BiFeO₃, such as magnetic,[6] electrical, and optical properties, among others. Only a very few works have reported obtaining phase-pure BiFeO₃ particles.[7] In addition, the annealing of the samples at temperatures above 600 °C frequently generates the Bi₂Fe₄O₉ impurity. Besides the aforementioned drawbacks and the restrictions, it should be considered that when water is added to Bi(NO₃)₃·5H₂O it hydrolyzes and causes the formation of basic bismuth nitrates such as [Bi₆O₄(OH)₄](NO₃)₆·4H₂O, [Bi₆O₅(OH)₃](NO₃)₅·3H₂O, [Bi₆O₄(OH)₃](NO₃)₃·1.5H₂O, and others.[13−16] Unfortunately, to completely decompose those basic bismuth nitrates, it is necessary to heat the samples between 550 and 600 °C.[13,16] This means that the NO₃⁻ anions coming from the reagents and from the dissolved HNO₃ may be another problem for obtaining pure BiFeO₃ particles. Thus it is important to be aware of these inconveniences to avoid or reduce the formation of unwanted byproducts. One of the synthesis strategies to reduce the formation of impurities in solution combustion process is presented in the next paragraph.

Solution combustion reactions are exothermic redox reactions in which the NO₃⁻ anions are reduced to NO$_x$(g)

Table 1. Amounts of Reagents Used To Prepare Four BiFeO₃ Samples and the Oxidizing/Reducing Agent Ratio

name of the sample	Bi(NO₃)₃·5H₂O (g)	Fe(NO₃)₃·9H₂O (g)	glycine (g)	volume of HNO₃ (mL)	NO₃⁻ ions/glycine ratio	equivalence ratio (Φ_e)
BiFeO₃-10	0.9701	0.8113	0.3015	1.9	10	0.180
BiFeO₃-7.4	0.9701	0.8113	0.3015	1.2	7.4	0.243
BiFeO₃-5.2	0.9701	0.8113	0.3015	0.6	5.2	0.346
BiFeO₃-3.6	0.9701	0.8113	0.3750	0.4	3.6	0.501

or $N_2(g)$ by some organic molecules (called fuel or reducing agent) such as glycine, hexamethylene tetramine, and maleic hydrazide, among others.[17,18] Metal nitrates, HNO_3, and NH_4NO_3 are oxidizing agents, also called oxidizers.[18] In those reactions, the highest amount of energy is produced, and hence, the temperature reached by the combustion is the highest when the equivalence ratio (Φ_e) is equal to 1.[17] In the specific case of aqueous solutions that contain glycine and the other reagents used to obtain $BiFeO_3$, the Φ_e value is given by the following equation

$$\Phi_e = \big[(\text{number of moles of glycine}) \times (+9)\big]$$
$$/\big[(-1)\{[\text{number of moles of Bi}(NO_3)_3 + Fe(NO_3)_3]$$
$$\times (-15) + \text{number of moles of } HNO_3 \times (-5)\}\big]$$

The specific values included in the formula for obtaining Φ_e are related to the reducing and oxidizing valences of each compound. The reducing valence of the glycine molecule ($C_2H_5NO_2$) is +9 (+4 for each C, +1 for each H, 0 for N, and −2 for each O), and the oxidizing valences for $Bi(NO_3)_3 \cdot 5H_2O$, $Fe(NO_3)_3 \cdot 9H_2O$, and HNO_3 are −15, −15, and −5 per formula unit, respectively.[17] Accordingly, it worth synthesizing $BiFeO_3$ particles using different Φ_e values by systematically varying the volume of used HNO_3. Moreover, because the H^+ ions bond to both the carboxylate and the amino group of the glycine,[19] inhibiting the formation of coordination complexes between the glycine and the Bi^{3+} and Fe^{3+} cations, the volume of HNO_3 used must be small.

Considering the aforementioned issues, the objective of this work was to determine the effects of oxidizing/reducing agent ratio (and hence Φ_e) in the synthesis of $BiFeO_3$ particles, especially in the perspective of decrease in impurity concentration, improvement in magnetic properties, and change in morphology. It was found that the sample synthesized with the highest Φ_e value showed the highest magnetic moment and the lowest average particle size and was free from the $Bi_2Fe_4O_9$ impurity.

2. EXPERIMENTAL SECTION

2.1. Reagents and Equipment. The materials used were bismuth nitrate pentahydrate ($Bi(NO_3)_3 \cdot 5H_2O$, Sigma, 99.99%), iron nitrate nonahydrate ($Fe(NO_3)_3 \cdot 9H_2O$, Sigma, 99.99%), glycine (H_2NCH_2COOH, Aldrich, 99%), and diluted nitric acid (HNO_3, J. T. Baker, 66%). Powder X-ray diffraction (XRD) patterns of the samples were recorded in a D8 Discover X-ray diffractomer (Bruker) providing Cu Kα emission (wavelength λ = 1.5418 Å) as excitation radiation. Raman spectra of the samples were recorded in a LabRAM-HR spectrometer (HORIBA-Jobin Yvon), equipped with a He−Ne laser (λ = 632.8 nm). The diffuse reflectance spectra (DRS) used for the Kubelka−Munk analysis were recorded in a Cary-5000 spectrometer (Varian). Scanning electron microscopy (SEM) images were taken in a JEOL JSM-7800F field-emission scanning electron microscope operating at 3.0 kV. To prepare the samples for the SEM measurements, the powders were previously dispersed in ethanol inside an agate mortar and ground and then deposited on silicon substrates. A Wissel-Electronik Mössbauer spectrometer with ⁵⁷Co
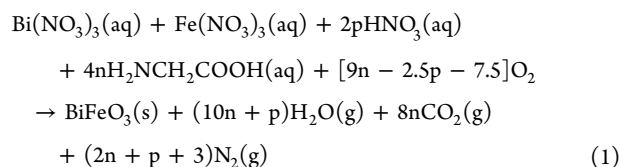
source embedded in an Rh matrix, operating at 300 K was utilized for recording the Mössbauer spectra of the samples. The data for each spectrum were collected for 30 h.

2.2. Synthesis of Submicroparticles. A typical preparation process used to obtain $BiFeO_3$ was as follows: In a 250 mL volume glass beaker, 2 mmol (0.9701 g) of $Bi(NO_3)_3 \cdot 5H_2O$, 2 mmol (0.8113 g) of $Fe(NO_3)_3 \cdot 9H_2O$, 4 mmol (0.3015 g) of glycine, 40 mL of deionized water, and finally 1.9 mL of HNO_3 (66%) were added. The amount of each reagent used to prepare four $BiFeO_3$ samples is presented in Table 1. When the glycine was added to the aqueous precursor solution, its color changed from light red to an intense reddish wine due to the formation of a complex between the zwitterion ($H_3N^+−CH_2−CH_2−COO^-$) and the Fe(III) cations. However, when the HNO_3 was added and dissolved in the solution, the reddish wine color of the solution faded considerably. The observed color change occurred because of bonding of the generated $[H_3O^+]$ ions with the carboxylate group of the zwitterion and consequent partial destruction of the previously formed zwitterion−Fe(III) cation complex. The lowest volume of HNO_3 used was 0.4 mL because with this volume the 0.9701 g of $Bi(NO_3)_3 \cdot 5H_2O$ used was completely dissolved in water when roughly 30 mL of water was evaporated.

The mixture was magnetically stirred and heated to evaporate the water. Inasmuch as the H_2O in the beaker diminished, the pH of the mixture solution decreased and the $Bi(NO_3)_3 \cdot 5H_2O$ was dissolved completely. Once the water was completely evaporated, a viscous solid was formed and a combustion reaction occurred. During the combustion a small amount of brown NO_x, CO_2, H_2O, and N_2 gases evolved. Because of the combustion reaction, a fluffy brown powder was obtained. Moreover, a flame was observed inside the beaker during the combustion. The highest flame was for the sample prepared with the lowest oxidizing agent (nitrate ions)/reducing agent (glycine) ratio (i.e., for the BiFeO₃-3.6 sample). The temperature of the water during its evaporation was ∼85 °C. Conversely, the flame for the BiFeO₃-10 sample was hardly observed.

Then, the powder was annealed in an alumina crucible at 350 °C for 2 h and then at 500 °C for 2 h; after that it was cooled to room temperature. The heating rate used to attain the 350 and 500 °C temperatures was 10 °C/min. Finally, the powder was annealed at 600 °C for 3 h; the heating rate to increase the temperature from room temperature to 600 °C was 5 °C/min. All of these annealing processes were performed in an ambient (air) atmosphere. The powder samples were ground in an agate mortar and stored in glass vials under a N_2 atmosphere to displace the CO_2 present in the headspace. Finally, the cap of the vial was covered with parafilm and Teflon tape.

Considering the above observations, the balanced chemical reaction can be presented as eq 1. Nonetheless, because of the incomplete reduction of the nitrates ions, NO_x gases are also evolved. The number of moles of glycine and nitric acid used for each mole of $Bi(NO_3)_3 \cdot 5H_2O$ is designated with the n and p coefficients, respectively.

$$Bi(NO_3)_3(aq) + Fe(NO_3)_3(aq) + 2pHNO_3(aq)$$
$$+ 4nH_2NCH_2COOH(aq) + [9n - 2.5p - 7.5]O_2$$
$$\rightarrow BiFeO_3(s) + (10n + p)H_2O(g) + 8nCO_2(g)$$
$$+ (2n + p + 3)N_2(g) \tag{1}$$

3. RESULTS AND DISCUSSION

During continuous heating of the reaction mixture, its water content reduced (due to evaporation) and its red color progressively intensified, while the pH of the solution gradually increased.

3.1. X-ray Diffraction. As can be seen in Figure 1, both the intensity and position of the XRD peaks of all four samples
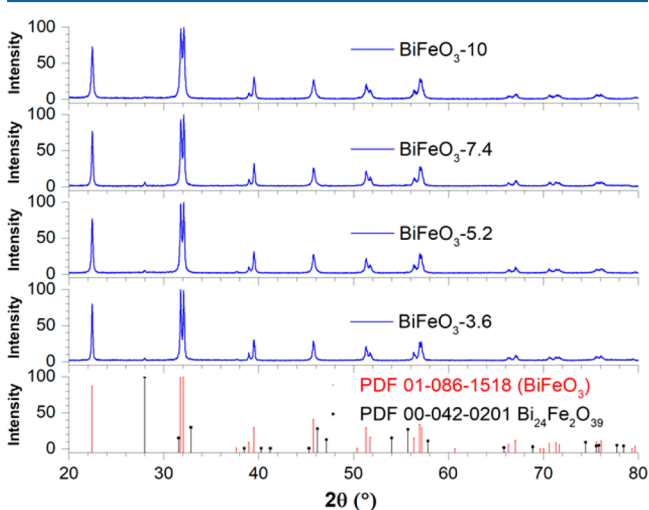

Figure 1. X-ray diffraction patterns of $BiFeO_3$ synthesized using four oxidizing/reducing agent ratios, annealed up to 500 °C. The intensity of the diffraction peaks in all of the spectra was normalized to the peak located at $2\theta = 32.08°$.

match well with the standard diffraction pattern of $BiFeO_3$ (vertical lines corresponding to the PDF no. 01-086-1588), indicating the formation of $BiFeO_3$ in rhombohedral phase. The full width at high-maximum (fwhm) and average crystallite size estimated using the Scherrer relation[20] for the four samples are presented in Table 2. Because the highest amount of NO_3^-

Table 2. fwhm and XRD Estimated Average Crystallite Size (nm) for the Four $BiFeO_3$ Samples Annealed up to 500 °C

sample	peak associated with (012) plane		peak associated with (024) plane	
	fwhm	crystallite size	fwhm	crystallite size
$BiFeO_3$-10	0.22	40	0.26	34
$BiFeO_3$-7.4	0.16	53	0.18	50
$BiFeO_3$-5.2	0.18	56	0.18	50
$BiFeO_3$-3.6	0.14	60	0.17	53

ions was present in the aqueous solution used for the synthesis of the $BiFeO_3$-10 sample, it is expected that after the combustion reaction the largest number of NO_3^- ions bonded to the Bi^{3+} and Fe^{3+} cations remain in the solid. Those NO_3^- anions bonded to Bi^{3+} cations do not decompose at 350 °C.[13] During the annealing of the sample at 500 °C, while the size of the $BiFeO_3$ crystallites grows, NO_3^- anions start to decompose. On the contrary, a smaller number of NO_3^- ions was used in the aqueous solution for the preparation of $BiFeO_3$-3.6 sample. The number of NO_3^- ions was also lowest in the combustion product due to the use of a greater amount of reducing agent as well as the higher temperature generated by the flame that promotes the decomposition of nitrate ions. A low NO_3^- ion

content hindered the growth of $BiFeO_3$ crystallites during the annealing of the powder at 500 °C.

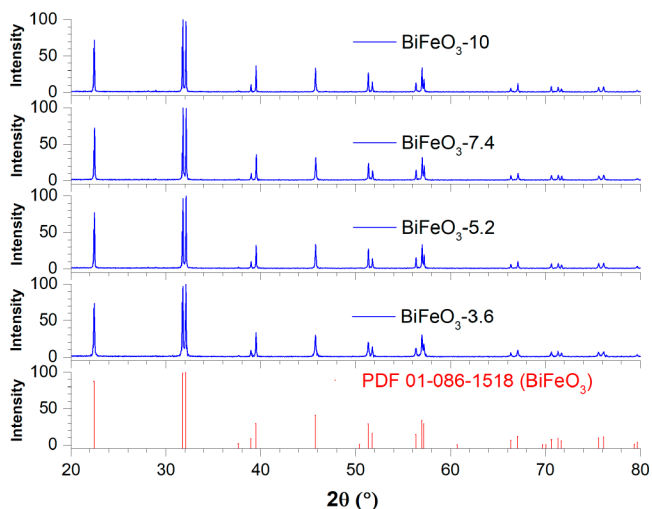The XRD patterns of the $BiFeO_3$ samples further annealed at 600 °C are presented in Figure 2. The patterns solely

Figure 2. X-ray diffraction patterns of $BiFeO_3$ synthesized using four oxidizing/reducing agent ratios, annealed up to 600 °C. The intensity in all patterns is normalized to the peak at $2\theta = 32.08°$.

correspond to the $BiFeO_3$ phase. Owing to this reannealing at 600 °C, the average crystallite size of the $BiFeO_3$ particles increases and, consequently, the width of the diffraction peaks (Figure 2) became narrower. For instance, the splitting of the peaks at $2\theta = 32.08°$ is more evident in samples annealed at 600 °C than at 500 °C. In Figure 3, amplifications of Figures 1 and 2 around $2\theta = 28°$ are shown, where the peaks of very low intensity associated with impurities are located. As can be noticed in Figure 3a, only a very weak diffraction peak located at $2\theta = 27.98°$ appeared, which does not correspond to $BiFeO_3$ oxide. This diffraction peak may be associated with small nanoparticles (NPs) of the byproduct $Bi_{24}Fe_2O_{39}$, although further experimental evidence is required to confirm this claim. Interestingly, when the samples were annealed at 600 °C, this byproduct was no longer present (see Figure 3b). In Figure 3b, there appeared two tiny diffraction peaks located at $2\theta = 28.16$ and 28.93° that correspond to the byproduct $Bi_2Fe_4O_9$ (PDF 00-072-1832). Note that the $Bi_2Fe_4O_9$ impurity was not detected for the $BiFeO_3$-3.6 sample, which is very important. Likewise, Köferstein obtained $BiFeO_3$ NPs with low impurity contents by decreasing the oxidizing/reducing agent ratio,[21] although the reducing agents used by the author were starch and acetic acid. The addition of HNO_3 in the reaction mixture was seen to increase the percentage of $Bi_2Fe_4O_9$ and $Bi_{25}FeO_{40}$ impurities up to 11%.

3.2. Raman and ATR-FTIR Spectroscopies. The Raman spectra presented in Figure 4a confirmed the sole presence of $BiFeO_3$ phase in the samples annealed up to 600 °C.[22] The position and corresponding vibrational mode associated with each of the bands are indicated (Figure 4a). As can be noticed, there is no additional band associated with any other phase or impurity in the Raman spectra, confirming the phase purity of the prepared samples. ATR-FTIR spectra of the samples were recorded in the 650–2000 cm^{-1} spectral range to ascertain their phase purity further (Figure 4b). While the appearance of a near-IR band around 814 cm^{-1} confirms the presence of the
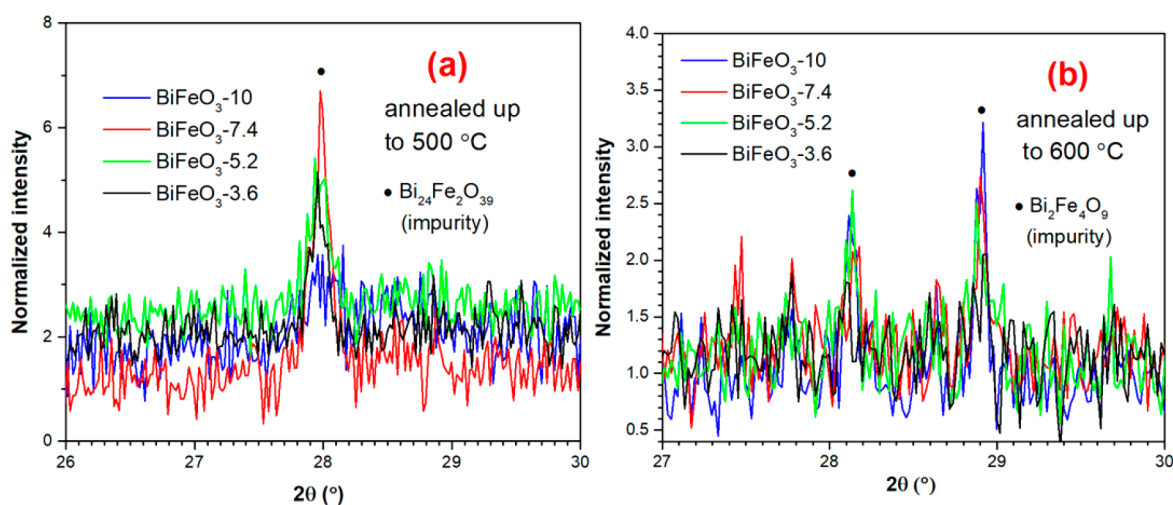
Figure 3. X-ray diffraction patterns in the range 2θ of 26−30°, for BiFeO$_3$ samples synthesized using four oxidizing agent/reducing agent ratios. The intensity in all patterns is normalized to 100 with the peak at $2\theta = 32.08°$.
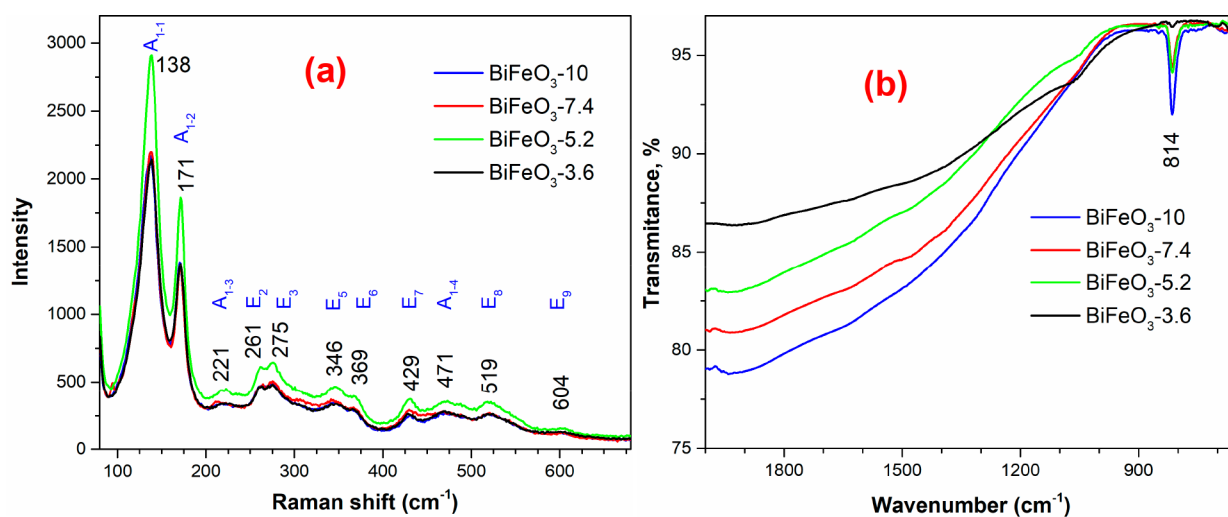

Figure 4. (a) Raman and (b) ATR-FTIR spectra of BiFeO$_3$ samples synthesized using four oxidizing/reducing agent ratios and annealed up to 600 °C.
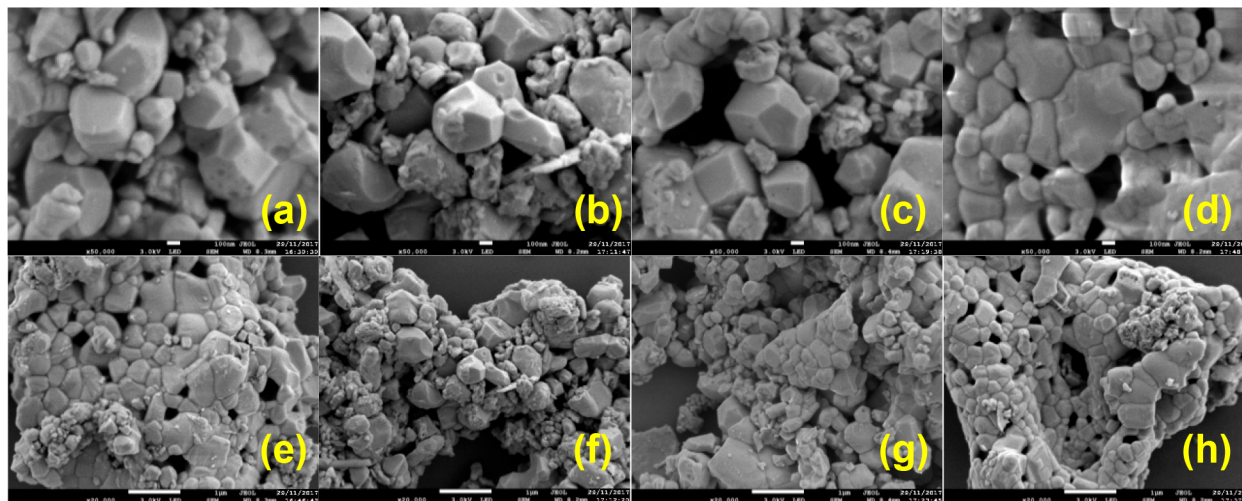

Figure 5. Typical SEM images of BiFeO$_3$ samples synthesized using four oxidizing/reducing agent ratios: 10 (a,e), 7.4 (b,f), 5.2 (c,g), and 3.6 (d,h). The length of the scale bar in panels a−d is 100 nm, whereas in panels e−h it is 1 μm. The samples were annealed up to 600 °C.

$Bi_2Fe_4O_9$ byproduct[23] in the samples synthesized at oxidizing/reducing agent ratio of 10, 7.4, and 5.2, the band is almost absent for the sample synthesized at the oxidizing/reducing agent ratio of 3.6. It must be noted that no signal associated with NO_3^- ions bonded to the Bi^{3+} or Fe^{3+} cations appeared in these samples.

3.3. Scanning Electron Microscopy.
Typical scanning electron microscopy (SEM) images of the four $BiFeO_3$ samples annealed up to 600 °C are presented in Figure 5. The formation of well-faceted $BiFeO_3$ crystallites in the few nanometers to few hundreds of nanometers size range is clear from the micrographs. As can be observed, $BiFeO_3$ samples synthesized with the oxidizing/reducing agent ratio of 10, 7.4, and 5.2 contain particles of wider size dispersion, containing very small particles (of a few nanometers size) along with bigger (of a few hundreds of nanometers size) ones, in contrast with the sample ($BiFeO_3$-3.6) fabricated at oxidizing/reducing agent ratio of 3.6. Apparently the smaller particles were not accommodated or agglomerated with the bigger ones during sintering. The absence of crystal facets and the fluffy nature of the smaller particles probably are the reasons for incomplete sintering or nonaccommodation of smaller particles with the bigger ones in these three samples. In contrast, particles of relatively smaller sizes with well-defined grain boundaries were formed in the sample $BiFeO_3$-3.6 prepared using oxidizing/reducing agent ratio of 3.6 (Figure 5d,h). Also, only a few smaller fluffy particles in this sample appeared to be unattached or unaccommodated with neighboring particles.

This fluffy material probably comes from the decomposition of basic bismuth nitrates produced by the nitrates ions in excess, which were not reduced to NO_x or N_2 by the glycine. The higher flame and temperature attained within the solution during the combustion for the sample prepared at the oxidizing/reducing agent ratio of 3.6 helped not only to enhance the crystallinity of $BiFeO_3$ particles but also to improve their stoichiometry. It should be recalled that the byproduct $Bi_2Fe_4O_9$ was not detected by the XRD or ATR-FTIR techniques in this sample. The average particles sizes (ca.) estimated from Figure 5e−h (without considering fluffy materials) were 284, 326, 251, and 246 nm, respectively.

3.4. Diffuse Reflectance Spectroscopy.
The Kubelka−Munk (K−M) transformed diffuse reflectance spectra of the $BiFeO_3$ samples annealed up to 600 °C are presented in Figure 6. While a well-defined absorption edge around 550 nm could be noted for all four samples, the shape of the K−M function of the $BiFeO_3$-3.6 sample is quite different from the others in the 600−750 nm range. The difference might be due to the presence of amorphous material or impurities such as γ-Fe_2O_3 in small quantities. Corresponding plots used to determine the direct and indirect band gap of the samples are depicted in Figures 7. The direct band gap energy of all of these samples remained between 2.19 and 2.12 eV. Apart from the direct transition, three indirect transitions could be detected for each of the samples. Estimated band gap energy corresponding to the first (E_g^{i1}), second (E_g^{i2}), and third (E_g^{i3}) indirect transitions varied between 1.71 and 1.88 eV, 1.22 and 1.35 eV, and 1.01 and 1.05 eV, respectively (Figure 7). According to the band structure obtained by theoretical calculations,[24,25] indirect electronic transitions in $BiFeO_3$ occur between 1.77 and 2.6 eV. However, there exist only a few experimental reports on the energy position of indirect transitions of $BiFeO_3$.[11,26,27] The reported energy values are 1.84,[26] 2.1,[27] and 1.65 eV.[11] It is worth mentioning that previous works on
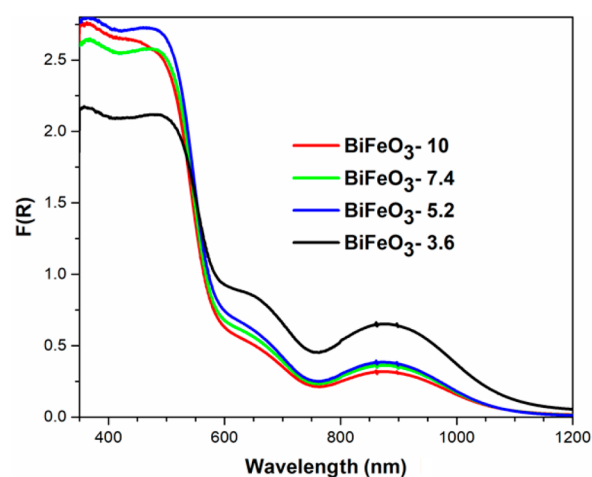

Figure 6. Kubelka−Munk-transformed reflectance spectra of $BiFeO_3$ samples synthesized using four oxidizing/reducing agent ratios and annealed up to 600 °C.

$BiFeO_3$ reported reflectance spectra only between 200 and 800 nm.

3.5. Vibrating Sample Magnetometry.
The room-temperature magnetization curves (Figure 8a) along with zero-field-cooled (ZFC) and field-cooled (FC) magnetization (Figure 8b) of the $BiFeO_3$ samples prepared at different oxidizing/reducing agent ratios and annealed up to 600 °C are presented in Figure 8. The ZFC and FC curves were recorded in between 1.8 and 300 K under an applied magnetic field of 500 Oe. As can be seen in Figure 8a, the shapes of the magnetization curves corresponding to the $BiFeO_3$-10, $BiFeO_3$-7.4, and $BiFeO_3$-5.2 samples are typical of an antiferromagnetic material. In contrast, the magnetization curve of the $BiFeO_3$-3.6 sample has the shape of an antiferromagnetic material superimposed over a superparamagnetic or a ferromagnetic material. The existence of ferromagnetic ordering in these particles was confirmed through the estimation of the coercive field at different temperatures, as presented in Table 3. The coercivity of all of the samples increased with the decrease in temperature, as occurs in ferromagnetic materials such as polycrystalline FePt clusters sintered at 1273 K.[28] Nevertheless, the values of the coercive fields are very low. It was found that as the oxidizing/reducing agent ratio decreases, the coercive field at lower temperatures increases, although this trend was not maintained for the sample $BiFeO_3$-3.6 beyond 200 K.

As can be seen in Figure 8, in general, the magnetic moment of $BiFeO_3$ particles increases with the decrease in oxidizing/reducing agent ratio. The magnetic moment of the $BiFeO_3$-3.6 sample is considerably higher than that of the other three $BiFeO_3$ samples. The increase in magnetization in bismuth ferrite NPs has been attributed to the contribution of uncompensated spins at the surface, strain anisotropy, and noncollinear magnetic ordering.[7] As can be seen in Figure 5a−d, the $BiFeO_3$-3.6 sample consists of well-crystalline submicroparticles of ~100 nm size, which favors the increase in magnetization by uncompensated spins at the surface or grain boundaries. Moreover, because the spins in $BiFeO_3$ particles are not perfectly antiparallel (i.e., not completely antiferromagnetic), a net magnetic moment arises due to this spin alignment. Specifically, within a $BiFeO_3$ particle, the net magnetic moment cancels out each 62 nm (i.e., the period of the spin cycloid).[29] Therefore, smaller $BiFeO_3$ particles
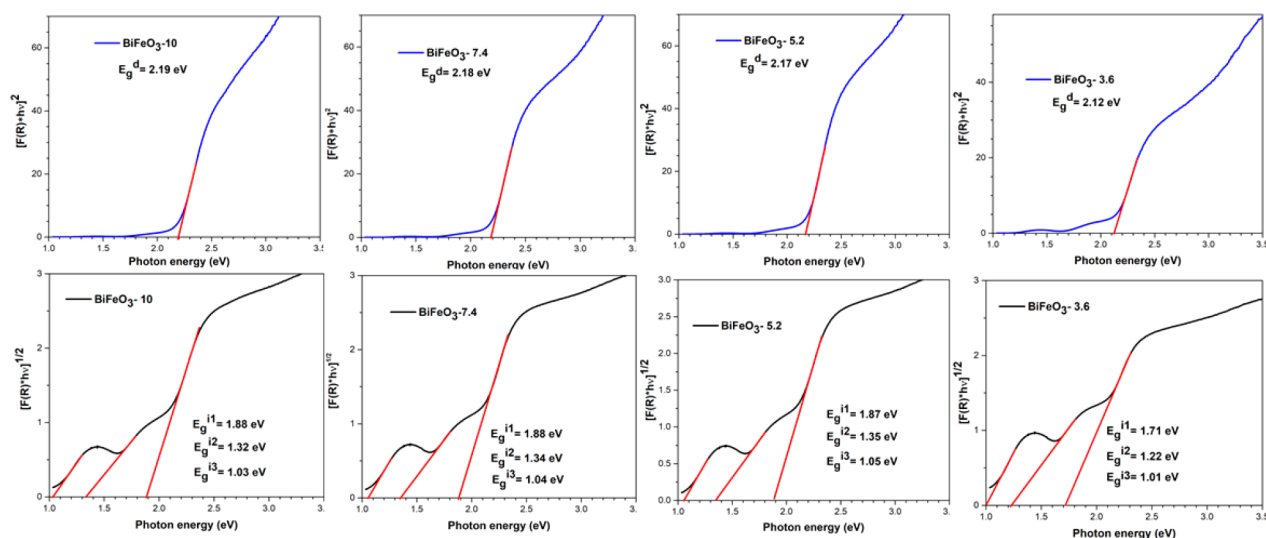
Figure 7. K−M plots used to estimate band gap energy (E_g) of the $BiFeO_3$ samples synthesized using four oxidizing/reducing agent ratios and annealed up to 600 °C.
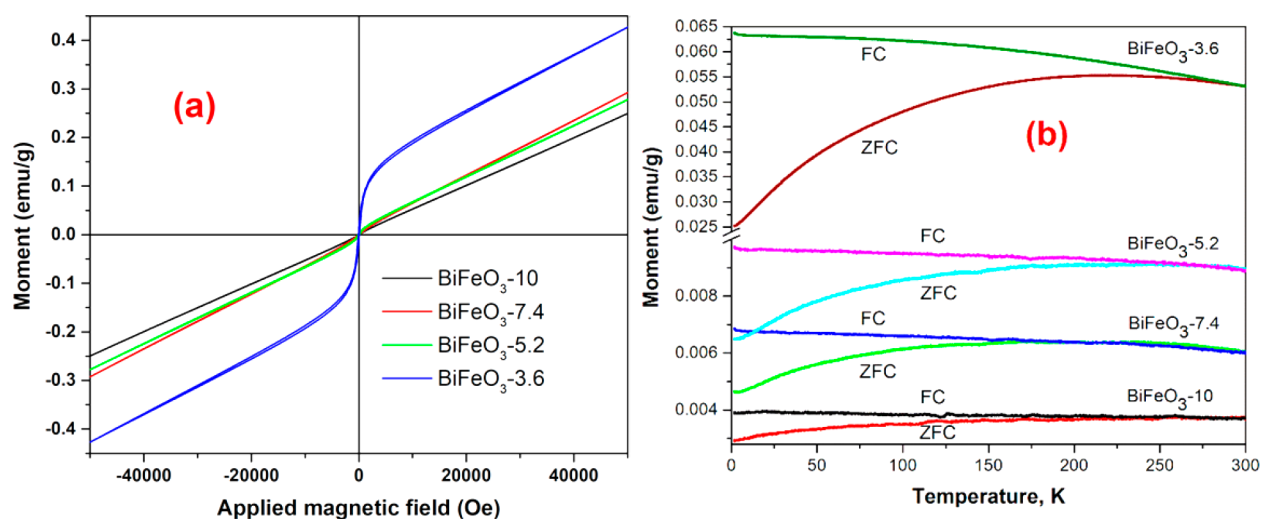

Figure 8. (a) Magnetization versus applied magnetic field curves at 300 K and (b) zero-field-cooled (ZFC) and field-cooled (FC) magnetization curves (under 500 Oe applied magnetic field) for the $BiFeO_3$ samples synthesized using different oxidizing/reducing agent ratios and annealed up to 600 °C.

Table 3. Coercive Fields (Oe) of the $BiFeO_3$ Samples Synthesized at Different Oxidizing/Reducing Agent Ratios and Annealed up to 600 °C, Estimated at Different Temperatures

sample	1.8 K	60 K	coercive field at 100 K	200 K	300 K
$BiFeO_3$-10	734	330	185	108	80
$BiFeO_3$-7.4	1207	484	284	178	172
$BiFeO_3$-5.2	1226	692	529	353	288
$BiFeO_3$-3.6	1561	827	594	321	198

contribute more to the net magnetic moment than larger particles. This is the reason for the $BiFeO_3$-3.6 sample exhibiting the highest magnetic moment (Figure 8a). It is worth recalling that the amorphous $BiFeO_3$ has a spin-glass behavior.[30] Likewise, the surface of the $BiFeO_3$ submicroparticles and the fluffy material present in our samples (Figure 5) should behave similar to amorphous $BiFeO_3$. The reported room-temperature (295 K) magnetization of amorphous $BiFeO_3$ is ∼0.5 emu/g.[30] As can be noticed in Figure 8a, this

magnetization of 0.5 emu/g is slightly higher than the magnetization for $BiFeO_3$ submicroparticles fabricated using the oxidizing/reducing agent ratio of 3.6. Finally, the room-temperature (300 K) magnetization values of the phase-pure $BiFeO_3$-10, $BiFeO_3$-7.4, and $BiFeO_3$-5.2 samples (annealed up to 600 °C) under 5.0 T applied magnetic field varied between 0.25 and 0.3 emu/g, which is slightly lower than the reported magnetization value for bulk $BiFeO_3$ (i.e., 0.34 emu/g).[7] However, in the preparation of that bulk $BiFeO_3$ sample, the authors used Fe_2O_3 as reactant, and they also used a multiple-step nitric acid (17%) leaching process that could dissolve the surface of $BiFeO_3$ and generate impurities such as Fe_2O_3.[7]

However, the possible presence of superparamagnetic γ-Fe_2O_3 NPs undetected by XRD and Raman analysis can also increase the magnetization of the fabricated $BiFeO_3$ submicroparticles. In fact, Lopes et al. detected an increase in magnetization in their paramagnetic $Bi_{25}FeO_{39}$ of submicrometric dimensions due to the presence of γ-Fe_2O_3, α-Fe_2O_3, or Fe_3O_4 impurities undetected by XRD.[31] The possible

contribution of γ-Fe_2O_3 impurity makes sense due to following two reasons: First, the magnetization of γ-Fe_2O_3 at 50 000 Oe is 44 emu/g,[31] and hence a small amount of this impurity (e.g., 0.5 wt %) can change the 0.3 emu/g magnetization value reported for $BiFeO_3$ particles. Second, γ-Fe_2O_3 NPs with sizes <25 nm are superparamagnetic at room temperature.[31]

The temperature where the ZFC and FC curves visibly split is qualitatively defined as the splitting temperature.[32] While the $BiFeO_3$ sample synthesized with oxidizing/reducing agent ratio of 10 ($BiFeO_3$-10) did not reveal a well-defined splitting temperature, the splitting temperatures for the samples synthesized with oxidizing/reducing agent ratios of 7.4, 5.2, and 3.6 were estimated to be 167, 240, and 280 K, respectively. Park et al.[7] have reported a size-dependent splitting temperature for multiferroic $BiFeO_3$ particles, finding around 150 and 300 K for 75 and 245 nm $BiFeO_3$ particles, respectively. In our case, the $BiFeO_3$-3.6 sample exhibited the highest splitting temperature, probably due to its superior crystallinity and the absence of the byproduct $Bi_2Fe_4O_9$. Previous works dealing with $BiFeO_3$ magnetic properties attributed the splitting between the ZFC and FC curves to spin-glass type behavior of $BiFeO_3$ particles.[7,33−35] The ZFC curves of our $BiFeO_3$ submicroparticles (Figure 8b) did not reveal well-defined maximum, probably due to the spin-glass behavior and broad size distribution of their particles, as shown in Figure 5.

Because $BiFeO_3$ belongs to the group of orthoferrites, it is worth comparing its magnetic properties with other orthoferrites. Thin films of hexagonal orthoferrites $RFeO_3$ (R = Lu, Er−Tb) are reported to exhibit weak ferromagnetism below 120−140 K.[36] Also, in $LaFeO_3$ and $YFeO_3$, the presence of a Dzyaloshinskii−Moriya (DM) interaction induces a canting of spin−lattice, generating weak ferromagnetism.[37] It is also worth comparing its magnetic properties with one of the most studied ferrites, that is, $CoFe_2O_4$. The temperature at which the NPs change from ferromagnetic to superparamagnetic order is known as blocking temperature (T_B). According to Ajroudi et al.,[38] the T_B for 6.8 nm $CoFe_2O_4$ NPs is 300 K. For 150 nm $BiFeO_3$ particles, the change from antiferromagnetic to paramagnetic order is between 600 and 640 K as was evidenced by Mössbauer spectroscopy.[29] According to Ammar et al.,[39] 5 nm $CoFe_2O_4$ NPs obtained by four different synthesis methods exhibited T_B values of 300, 235, 180, and 60 K. Those differences in T_B were attributed to the shape and size of the particles, their degree of agglomeration, and the volume and surface defects. As can be seen from the ZFC curves (Figure 8b), the $BiFeO_3$ samples did not reveal a clear maximum in the measured temperature range.

3.6. ^{57}Fe Mössbauer Spectroscopy. The small amount of fluffy material (Figure 5) present in the synthesized samples is poorly crystallized and hence can exhibit paramagnetic behavior. In contrast, well-crystalline $BiFeO_3$ submicroparticles exhibit antiferromagnetic behavior. Therefore, we performed the room-temperature Mössbauer spectroscopy on two representative samples ($BiFeO_3$-3.6 and $BiFeO_3$-10) annealed up to 600 °C to quantify the percentage of material in each sample that exhibits paramagnetic behavior. The experimental and fitted Mössbauer spectra of the two $BiFeO_3$ samples are shown in Figure 9. The six-band spectra (sextet) with isomer shift (δ) at ~0.27 mm/s originated from the Fe^{3+} cations located in an antiferromagnetic environment (i.e., in crystalline $BiFeO_3$ submicroparticles). The asymmetry in intensity of the sextet stems from an intrinsic anisotropy of the magnetic hyperfine interaction at a site with trigonal symmetry.[40] A
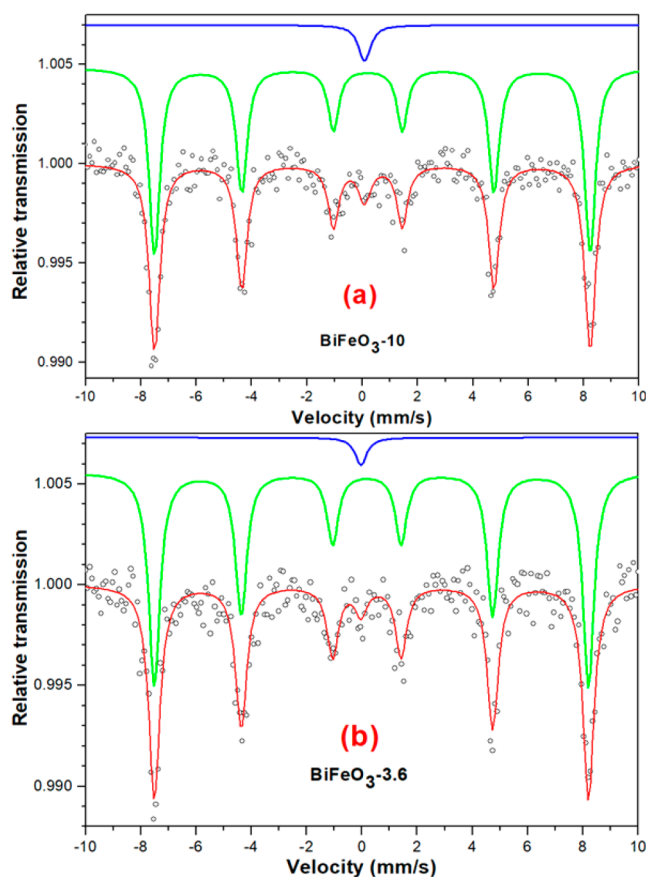

Figure 9. Mössbauer spectra of the $BiFeO_3$ samples synthesized using two different oxidizing/reducing agent ratios (10 and 3.6). The samples were annealed up to 600 °C. While the empty circles correspond to experimental data points, the blue and green curves correspond to the Lorentzian deconvolutions of experimental spectra.

model to account for that asymmetry was develop by Landers et al.[29] From the relative areas associated with the sextets indicated in Table 4, it is deduced that approximately 95−97%

Table 4. Mössbauer Hyperfine Parameters of the Fitted Spectra for the $BiFeO_3$ Submicroparticles Shown in Figure 9

sample	Fe species	δ (mm/s)	Δ (mm/s)	Bhf (kOe)	relative area (%)
$BiFeO_3$-10	sextet	0.28	0.16	488	94.9
	singlet	0.08			5.1
$BiFeO_3$-3.6	sextet	0.26	0.16	487	96.7
	singlet	0.01			3.3

of the Fe^{3+} cations in the samples are located in antiferromagnetic sites of the $BiFeO_3$ lattice. The area fractions of the singlet located at $\delta \approx 0$ mm/s were 5.1 and 3.3% of the experimental spectral area for the $BiFeO_3$-10 and $BiFeO_3$-3.6 samples, respectively (Table 4). These results are consistent with the observations made from the SEM micrographs (Figure 5) that the $BiFeO_3$-3.6 sample has the smallest amount of fluffy material. As has been reported by Tanaka et al.,[41] ^{57}Fe-enriched $BiFeO_3$ thin films also reveal a singlet at $\delta \approx 0$ mm/s in their Mössbauer spectra. The area of the singlet in their films was ~18%. When the spectra were measured at the velocity range of only ±2.8 mm/s, the singlet turned to be a paramagnetic doublet.[41] According to Tanaka et al., the presence of material

with paramagnetic behavior affects the room-temperature electrical properties of BiFeO$_3$.[41] This discussion is very useful in the present context, especially for the researchers who intend to use BiFeO$_3$ in electrocatalysis because the presence of such a small fraction of paramagnetic material can modify the electrocatalytic activity or electrical properties of well-crystalline BiFeO$_3$.

4. CONCLUSIONS

We demonstrate the fabrication of phase-pure BiFeO$_3$ particles through solution combustion reaction process using glycine as a reducing agent and metal nitrates and nitric acid as oxidizing agents. By adjusting the oxidizing/reducing agent ratio to 3.6, which corresponds to an oxidizing/reducing agent equivalence ratio (Φ_e) close to 0.5, it was possible to avoid the formation of common impurity phases such as Bi$_2$Fe$_4$O$_9$ in the samples. The adjustment of Φ_e and subsequent air annealing at optimum temperature (600 °C) also reduces the formation of fluffy, amorphous materials of undefined shapes around the well-defined BiFeO$_3$ particles. The room-temperature magnetic moment of the phase-pure BiFeO$_3$ particles synthesized at oxidizing/reducing agent ratio of 3.6 is almost twice that of the BiFeO$_3$ particles synthesized at oxidizing/reducing agent ratios of 10, 7.4, and 5.2, indicating a huge improvement in magnetic properties due to the elimination of unwanted impurities, smaller average particle size, and superior crystallinity. Moreover, the phase-pure BiFeO$_3$ particles manifest higher splitting temperature between their ZFC and FC magnetization curves and moderate coercive field, manifesting their stable anti-ferromagnetic behavior over a wide temperature range (2−300 K). The highly faceted crystalline structure, adequate bad gap energy, and weak ferromagnetic behavior at low magnetic field of the phase-pure BiFeO$_3$ particles make them their application as magnetically separable visible-light photocatalysts attractive. The superparamagnetic behavior in one sample of BiFeO$_3$ may be originated by impurities attached to the BiFeO$_3$.

■ AUTHOR INFORMATION

Corresponding Author
*E-mail: upal@ifuap.buap.mx.

ORCID ⓘ
Umapada Pal: 0000-0002-5665-106X

Author Contributions
The manuscript was written through contributions of all authors. All authors have given approval to the final version of the manuscript.

Notes
The authors declare no competing financial interest.

■ ACKNOWLEDGMENTS

■ REFERENCES

(1) Catalan, B. G.; Scott, J. F. Physics and Applications of Bismuth Ferrite. *Adv. Mater.* **2009**, *21*, 2463−2485.

(2) Niu, F.; Gao, T.; Zhang, N.; Chen, Z.; Huang, Q.; Qin, L.; Sun, X.; Huang, Y. Hydrothermal Synthesis of BiFeO$_3$ Nanoparticles for Visible Light Photocatalytic Applications. *J. Nanosci. Nanotechnol.* **2015**, *15*, 9693−9698.

(3) McDonnell, K.; Wadnerkar, N.; English, N. J.; Rahman, M.; Dowling, D. Photo-Active and Optical Properties of Bismuth Ferrite (BiFeO$_3$): An Experimental and Theoretical Study. *Chem. Phys. Lett.* **2013**, *572*, 78−84.

(4) Singh, H.; Rajput, J. K. Chelation and Calcination Promoted Preparation of Perovskite-Structured BiFeO$_3$ Nanoparticles: A Novel Magnetic Catalyst for the Synthesis of Dihydro-2-Oxypyrroles. *J. Mater. Sci.* **2018**, *53*, 3163−3188.

(5) Selbach, S. M.; Tybell, T.; Einarsrud, M.; Grande, T. Size-Dependent Properties of Multiferroic BiFeO$_3$ Nanoparticles. *Chem. Mater.* **2007**, *19*, 6478−6484.

(6) Lu, J.; Günther, A.; Schrettle, F.; Mayr, F.; Krohns, S.; Lunkenheimer, P.; Pimenov, A.; Travkin, V. D.; Mukhin, A. A.; Loidl, A. On the Room Temperature Multiferroic BiFeO$_3$: Magnetic, Dielectric and Thermal Properties. *Eur. Phys. J. B* **2010**, *75*, 451−460.

(7) Park, T.; Papaefthymiou, G. C.; Viescas, A. J.; Moodenbaugh, A. R.; Wong, S. S. Size-Dependent Magnetic Properties of Single-Crystalline Multiferroic BiFeO$_3$ Nanoparticles. *Nano Lett.* **2007**, *7*, 766−772.

(8) Biasotto, G.; Simões, A.; Foschini, C.; Antônio, S.; Zaghete, M.; Varela, J. A Novel Synthesis of Perovskite Bismuth Ferrite Nano-particles. *Process. Appl. Ceram.* **2011**, *5*, 171−179.

(9) Kothai, V.; Ranjan, R. Synthesis of BiFeO$_3$ by Carbonate Precipitation. *Bull. Mater. Sci.* **2012**, *35*, 157−161.

(10) Lomanova, N. A.; Tomkovich, M. V.; Sokolov, V. V.; Gusarov, V. V. Special Features of Formation of Nanocrystalline BiFeO$_3$ via the Glycine-Nitrate Combustion Method. *Russ. J. Gen. Chem.* **2016**, *86*, 2256−2262.

(11) Ortiz-Quiñonez, J. L.; Díaz, D.; Zumeta-Dubé, I.; Arriola-Santamaría, H.; Betancourt, I.; Santiago-Jacinto, P.; Nava-Etzana, N. Easy Synthesis of High-Purity BiFeO$_3$ Nanoparticles: New Insights Derived from the Structural, Optical, and Magnetic Characterization. *Inorg. Chem.* **2013**, *52*, 10306−10317.

(12) Dash, P.; Dash, B. N.; Rath, H.; Rath, C.; Mishra, N. C. Evolution of Phase Purity and Texture on Annealing of BiFeO$_3$ Thin Film Prepared by Sol-Gel Technique. *Indian J. Phys.* **2009**, *83*, 485−491.

(13) Christensen, A. N.; Chevallier, M.; Skibsted, J.; Iversen, B. B. Synthesis and Characterization of Basic bismuth(III) Nitrates. *J. Chem. Soc., Dalt. Trans.* **2000**, 265−270.

(14) Lazarini, F. Bismuth Basic Nitrate [Bi$_6$(H$_2$O)(NO$_3$)O$_4$(OH)$_4$]-(NO$_3$)$_5$. *Acta Crystallogr., Sect. B: Struct. Crystallogr. Cryst. Chem.* **1979**, *35*, 448−450.

(15) Sundvall, B.; Elgsaeter, A.; Oftedal, G.; Strand, K. A.; Hoyer, E.; Spiridonov, V. P.; Strand, T. G. Crystal and Molecular Structure of Tetraoxotetrahydroxobismuth(III) Nitrate Monohydrate, Bi6O4-(HO)4(NO3)6.H2O. *Acta Chem. Scand.* **1979**, *33a*, 219−224.

(16) Henry, N.; Mentré, O.; Abraham, F.; MacLean, E. J.; Roussel, P. Polycationic Disorder in [Bi$_6$O$_4$(OH)$_4$](NO$_3$)$_6$: Structure Determination Using Synchrotron Radiation and Microcrystal X-Ray Diffraction. *J. Solid State Chem.* **2006**, *179*, 3087−3094.

(17) Patil, K. C.; Hegde, M. S.; Rattan, T.; Aruna, S. T. *Chemistry of Nanocrystalline Oxide Materials: Combustion Synthesis, Properties and Applications*; World Scientific Publishing Co.: Singapore, 2008.

(18) Varma, A.; Mukasyan, A. S.; Rogachev, A. S.; Manukyan, K. V. Solution Combustion Synthesis of Nanoscale Materials. *Chem. Rev.* **2016**, *116*, 14493−14586.

(19) Hancock, R. D.; Cukrowski, I.; Baloyi, J.; Mashishi, J. The Affinity of Bismuth (III) for Nitrogen-Donor Ligands. *J. Chem. Soc., Dalton Trans.* **1993**, 2895−2899.

(20) Langford, J. I.; Wilson, A. J. C. Scherrer after Sixty Years: A Survey and Some New Results in the Determination of Crystallite Size. *J. Appl. Crystallogr.* **1978**, *11*, 102−113.

(21) Köferstein, R. Synthesis, Phase Evolution and Properties of Phase-Pure Nanocrystalline $BiFeO_3$ Prepared by a Starch-Based Combustion Method. *J. Alloys Compd.* **2014**, *590*, 324−330.

(22) Yang, Y.; Sun, J. Y.; Zhu, K.; Liu, Y. L.; Chen, J.; Xing, X. R. Raman Study of $BiFeO_3$ with Different Excitation Wavelengths. *Phys. B* **2009**, *404*, 171−174.

(23) Zhao, J.; Liu, T.; Xu, Y.; He, Y.; Chen, W. Synthesis and Characterization of $Bi_2Fe_4O_9$ Powders. *Mater. Chem. Phys.* **2011**, *128*, 388−391.

(24) Ju, S.; Cai, T.-Y.; Guo, G.-Y. Electronic Structure, Linear, and Nonlinear Optical Responses in Magnetoelectric Multiferroic Material $BiFeO_3$. *J. Chem. Phys.* **2009**, *130*, 214708.

(25) Yaakob, M. K.; Taib, M. F. M.; Lu, L.; Hassan, O. H.; Yahya, M. Z. Self-Interaction Corrected LDA + U Investigations of $BiFeO_3$ Properties: Plane-Wave Pseudopotential Method. *Mater. Res. Express* **2015**, *2*, 116101.

(26) Fruth, V.; Tenea, E.; Gartner, M.; Anastasescu, M.; Berger, D.; Ramer, R.; Zaharescu, M. Preparation of $BiFeO_3$ Films by Wet Chemical Method and Their Characterization. *J. Eur. Ceram. Soc.* **2007**, *27*, 937−940.

(27) Huo, Y.; Jin, Y.; Zhang, Y. Citric Acid Assisted Solvothermal Synthesis of $BiFeO_3$ Microspheres with High Visible-Light Photocatalytic Activity. *J. Mol. Catal. A: Chem.* **2010**, *331*, 15−20.

(28) Stappert, S.; Rellinghaus, B.; Acet, M.; Wassermann, E. F. Gas-Phase Preparation of L10 Ordered FePt Nanoparticles. *J. Cryst. Growth* **2003**, *252*, 440−450.

(29) Landers, J.; Salamon, S.; Escobar Castillo, M.; Lupascu, D. C.; Wende, H. Mossbauer Study of Temperature-Dependent Cycloidal Ordering in $BiFeO_3$ Nanoparticles. *Nano Lett.* **2014**, *14*, 6061−6065.

(30) Nakamura, S.; Soeya, S.; Ikeda, N.; Tanaka, M. Spin-Glass Behavior in Amorphous $BiFeO_3$. *J. Appl. Phys.* **1993**, *74*, 5652−5657.

(31) Lopes, A. M. L.; Araújo, J. P.; Ferdov, S. Room Temperature Synthesis of $Bi_{25}FeO_{39}$ and Hydrothermal Kinetic Relations between Sillenite- and Distorted Perovskite-Type Bismuth Ferrites. *Dalt. Trans.* **2014**, *43*, 18010−18016.

(32) Buschow, K. H. J. *Handbook of Magnetic Materials*, 1st ed.; Elsevier: Amsterdam, 2015; Vol. 23.

(33) Jaiswal, a; Das, R.; Vivekanand, K.; Abraham, P. M.; Adyanthaya, S.; Poddar, P. Effect of Reduced Particle Size on the Magnetic Properties of Chemically Synthesized $BiFeO_3$ Nanocrystals. *J. Phys. Chem. C* **2010**, *114*, 2108−2115.

(34) Singh, M. K.; Prellier, W.; Singh, M. P.; Katiyar, R. S.; Scott, J. F. Spin-Glass Transition in Single-Crystal $BiFeO_3$. *Phys. Rev. B: Condens. Matter Mater. Phys.* **2008**, *77*, 1−5.

(35) Zhong, J.; Heremans, J. J.; Viehland, D.; Yee, G. T.; Priya, S. Ferromagnetism and Spin-Glass-like Behavior of $BiFeO_3$ Nanoparticles. *Ferroelectrics* **2010**, *400*, 3−7.

(36) Akbashev, A. R.; Semisalova, A. S.; Perov, N. S.; Kaul, A. R. Weak Ferromagnetism in Hexagonal Orthoferrites $RFeO_3$ (R = Lu, Er-Tb). *Appl. Phys. Lett.* **2011**, *99*, 122502.

(37) Coutinho, P. V.; Cunha, F.; Barrozo, P. Structural, Vibrational and Magnetic Properties of the Orthoferrites $LaFeO_3$ and $YFeO_3$: A Comparative Study. *Solid State Commun.* **2017**, *252*, 59−63.

(38) Ajroudi, L.; Mliki, N.; Bessais, L.; Madigou, V.; Villain, S.; Leroux, C. Magnetic, Electric and Thermal Properties of Cobalt Ferrite Nanoparticles. *Mater. Res. Bull.* **2014**, *59*, 49−58.

(39) Ammar, S.; Helfen, A.; Jouini, N.; Fiévet, F.; Rosenman, I.; Villain, F.; Molinié, P.; Danot, M. Magnetic Properties of Ultrafine Cobalt Ferrite Particles Synthesized by Hydrolysis in a Polyol Medium. *J. Mater. Chem.* **2001**, *11*, 186−192.

(40) Lebeugle, D.; Colson, D.; Forget, A.; Viret, M.; Bonville, P.; Marucco, J. F.; Fusil, S. Room-Temperature Coexistence of Large Electric Polarization and Magnetic Order in $BiFeO_3$ Single Crystals. *Phys. Rev. B: Condens. Matter Mater. Phys.* **2007**, *76*, 1−8.

(41) Tanaka, K.; Fujita, Y.; Okamura, S.; Yoshida, Y. Mössbauer Spectra and Electric Properties of ^{57}Fe-Enriched $BiFeO_3$ Thin Films. *Jpn. J. Appl. Phys.* **2014**, *53*, 09PA15.